Mott scattering in strong laser fields

C. Szymanowski,* V. Véniard, R. Taïeb, and A. Maquet
Laboratoire de Chimie Physique—Matière et Rayonnement, 11 rue Pierre et Marie Curie, Université Pierre et Marie Curie Paris VI, F-75 231 Paris Cedex 05, France

C. H. Keitel
Optics Section, Blackett Laboratory, Imperial College, London SW7 2BZ, United Kingdom
(Received 20 December 1996)

Qualitative and quantitative results of a complete relativistic calculation of the S-matrix transition amplitudes and first Born cross sections for the Mott scattering of an electron in the presence of an ultraintense single-mode laser field are compared in detail to a spinless and a nonrelativistic treatment. The role of the fermion character of the electron leading to spin-orbit and spin-laser interactions is discussed depending on the laser intensity and on the incoming electron kinetic energy. The differences between radiative transfer spectra of the electron energy in the relativistic and nonrelativistic regimes are addressed. [S1050-2947(97)00910-4]

PACS number(s): 34.80.Qb

I. INTRODUCTION

Even a slow electron, when submitted to an ultrastrong laser pulse, can experience significant relativistic effects. This statement bases on the qualitative argument that the averaged quiver energy $U_p = E^2/4\omega^2$ acquired by a classical electron within a linear polarized laser field with frequency ω can become comparable to its rest energy at high-field strength E. Recently developed ultraintense femtosecond laser sources [1] deliver pulses of near-infrared radiation with intensities such that U_p can well exceed c^2, and make it feasible to explore this regime occurring at about 10^{18} W/cm^2.

Calculations related to the radiative processes experienced by free electrons inside a strong electromagnetic field were worked out since the advent of laser sources in the early 1960s [2,3]. A treatment of Compton scattering in an intense electromagnetic field can even be found in the textbook by Berestetzkiĭ, Lifshitz, and Pitaevskiĭ [4]. It is, however, only recently that relativistic aspects of laser-induced processes have attracted a renewed interest, as a result of important advances in laser technology which have made possible to attain the required ultrahigh intensities. First experiments in which relativistic effects are clearly shown have been recently reported. The transition between Thomson and Compton scattering inside an ultraintense laser field was investigated in Ref. [5], and the influence of matter on light propagation in self-channeling in the relativistic regime in Ref. [6]. Experiments on nonlinear Compton scattering which were performed at SLAC were reported by Bula *et al.* [7]. Note that, in addition to the already mentioned early references, stimulated Compton scattering in more general than plane-wave fields was considered by Rosenberg [8]. The relation of ponderomotive forces and stimulated Compton scattering in the nonrelativistic limit was addressed in Ref. [9]. In addition, it has been known for a long time that free electrons inside a very strong laser field can emit high-order harmonic radiation, a problem which was investigated via a classical approach (see, for instance, Ref. [10]), and has been recently reported in experiments by Norreys *et al.* and von der Linde *et al.* [11].

Other types of laser-assisted processes, in which relativistic effecs are expected to be important, are the recently reported emission of energetic electrons and ions from atomic clusters submitted to ultrastrong infrared laser pulses [12]. In such a context, it is generally believed that, in the early stages of the process, the heating of the electrons released from atoms via multiphoton ionization results from stimulated inverse bremsstrahlung. The latter process takes place when the electrons are scattered from the neighboring ions, in the presence of the laser field. This observation has motivated the present study, in which we address the question of the importance of relativistic effects on laser-assisted Coulomb scattering, the so-called Mott scattering, in the high-intensity regime.

Regarding this class of laser-assisted electron-atom collisions, most theoretical studies have been restricted to the nonrelativistic domain [13,14]. It was soon realized and indeed experimentally verified that, as a general consequence of the infrared divergence of QED [15], quite a large number of photons can be exchanged between the field and the projectile-target system in the soft-photon limit, even at moderate field intensities [16]. On the other hand, relativistic simulations have been relatively scarce. Though Coulomb scattering for relativistic velocities was pioneered by Mott [17] in 1929, an extension of the first Born treatment [13] of laser-assisted Coulomb scattering to the relativistic domain has been formally derived by Denisov and Fedorov [19]. There has been an intricate covariant extension of the low-frequency Kroll-Watson results by Kamiński [20] using a nonlocal transformation into a generalized Kramers-Henneberger frame. The relativistic scattering inside a multimode radiation field was addressed by Zhou and Rosenberg [21] using a variational method, while the emission of bremsstrahlung in laser-assisted scattering in the low-frequency regime was considered by the same authors [22]. Recently, there have been analytical investigations of poten-

*Electronic address: szymanow@ccr.jussieu.fr

tial scattering of ultrarelativistic electrons in two codirectional lightwaves by Roshchupkin [23].

Let us also mention that several recent studies of relativistic effects were dedicated to understanding and modeling atomic multiphoton ionization in the domain of ultraintense laser fields. Classical Monte Carlo simulations of the ionization of atomic hydrogen were carried out by Keitel and Knight [24], where hot electron ejection was reported [25]. In the Kramers-Henneberger frame, relativistic mass shift effects on stabilization were recently investigated in Ref. [26]. A model of short-range potential for bosons was considered by Faisal and Radożycki [27], in order to provide analytic expressions for particle ejection, multiphoton absorption, and stimulated bremsstrahlung effects. Latinne, Joachain, and Dörr [28] investigated the Pauli equation in the regime of superintense electric fields in order to include first-order spin effects.

The main purpose of the present paper is to show that the modifications of the Mott scattering cross section for an electron in the Coulomb potential of a nucleus, in the presence of an ultraintense field, can provide interesting insights into questions of the importance and the signatures of the relativistic effects. We concentrate here on the underlying physics and the control of measurable quantities, meaning how relativity affects a typical atomic process. Our motivation for considering the spin-dependent relativistic Mott scattering is that the physics of this process can provide a clear distinction between simple kinematics and spin-orbit coupling effects. For this reason, we shall compare the results of a calculation of the (S-matrix) first Born approximation cross section for the Coulomb scattering of Dirac-Volkov electrons dressed by a circularly polarized laser field to the more simplified approach of spinless Klein-Gordon particles and to the corresponding nonrelativistic Schrödinger-Volkov treatment. The choice of Dirac-Volkov wave functions, modeling the state of a free electron embedded in a strong classical electromagnetic field, is well justified in view of the huge intensities considered for the laser. Indeed, in such laser fields, the occupation numbers of the modes are so large that spontaneous (Compton and bremsstrahlung) emission processes can be safely neglected, thus giving further credit to a classical description of the field. The breakdown of the validity of the model is expected to take place at intensities so high that pair creation (and also radiation reaction [18]) will come into play. This is not considered here.

We wish to mention that our relativistic Dirac-Volkov treatment is essentially the same as the one used by Denisov and Fedorov in their pioneering paper [19]. However, that work concentrated on deriving analytical approximate expressions for total cross sections under certain assumptions and specialized for linear polarization of the laser radiation. Here we shall instead consider the differential cross section in some detail, providing a physical interpretation of different contributions to the scattering matrix element. In order to avoid unnecessary complications in the analysis, we have chosen to treat the specialized case of a circularly polarized field. Then, as already noted by Denisov and Fedorov [19], the resulting expression of the amplitude becomes significantly more tractable than in the general case of elliptical polarization and even than for linear polarization. For circular polarization of the field, the transition amplitude can be expressed in terms of ordinary Bessel functions, whereas it contains more intricate generalized Bessel functions for other polarization states. This significantly simplifies the analysis of the results and the discussion of limiting cases, while retaining the essential of the physics of the process. Emphasis is placed on the energy distribution of the electrons after the scattering event, thus demonstrating the feasibility of obtaining particularly hot electrons as a result of collisions with large momentum transfer. The maximum attainable energy hereby turns out to depend chiefly on both the relativistic kinematics and the transient (quiver) energy of the particle aquired in the field. On the other hand, the spin-orbit coupling has an effect on the size of the cross section, which can change by up to about one order of magnitude, depending on whether or not it is included in the analysis. Finally, the angular distribution of the scattered electrons is displayed for several representative sets of parameters, comparing with simpler spinless relativistic and nonrelativistic approaches, in order to gain insight into the importance of the contributing physical processes. Our results show the importance of taking care of the fact that the electron is a fermion, especially in the case of ultraintense laser fields.

Note that in this work atomic units are used throughout. The velocity of light is $c \simeq 137$ a.u., while energy is measured in atomic units, 1 a.u.$\simeq$27.2116 eV. The atomic unit of intensity is 3.5×10^{16} W/cm^2 at the electrical field strength of $E=1$ a.u. For an angular frequency of $\omega=0.043$ a.u.$=1.17$ eV, corresponding to the lasing transition of the Nd laser at a wavelength of 1064 nm, for an intensity of about 10^{18} W/cm^2 or an electrical field strength of $E=5.89$ a.u., the ratio E/ω is of the order of c. This relativistic regime considered here is far below the intensity from which the electron will acquire such a high quiver momentum, so that enough energy will be available for pair creation in a collision process at about 10^{21} W/cm^2. Therefore, the description of the physical effects on one field-dressed electron is appropriate. Note that this intensity is again far below the intensity which makes the vacuum unstable against the creation of particle-antiparticle pairs. These effects are to be expected at about 10^{29} W/cm^2 according to Ref. [29].

The organization of this paper as follows: In Sec. II, we will present the formalism and establish the expression of the differential scattering cross section associated to the exchange of a given net number of laser photons. Section III is dedicated to a presentation of the corresponding expressions occurring when considering simplified treatments valid for spinless and nonrelativistic particles. Evidence of the role of spin interactions is presented in Sec. IV, where we also discuss the main qualitative features of the spectra, depending on the laser intensity, electron velocity, and angle of observation. The key points are summarized in a brief conclusion in Sec. V.

II. DIRAC-VOLKOV DIFFERENTIAL CROSS SECTION

A. Relativistic Volkov states

The relativistic electron with four-momentum p^μ inside a classical monochromatic electromagnetic field A^μ is described by a bispinor function ψ which obeys the Dirac equation

$$\left[\gamma^{\mu}\left(\hat{p}_{\mu}-\frac{A_{\mu}}{c}\right)-c\right]\psi=0, \tag{1}$$

where γ^{μ} are the Dirac matrices. They anticommute according to $\{\gamma^{\mu},\gamma^{\nu}\}=2g^{\mu\nu}$. The metric tensor of Minkowski space is $g^{\mu\nu}=\mathrm{diag}(1,-1,-1,-1)$. This starting point to deal with the dressing of the electron interacting with a classical field is adequate to treat the laser-assisted processes we have chosen to discuss here. More precisely, it is equivalent to assuming that multiphoton-stimulated bremsstrahlung (or multiphoton-stimulated emission) and multiphoton inverse bremsstrahlung (or multiphoton absorption) by far dominate the effects resulting from the coupling with the empty modes of the field. The solutions of the Dirac equation in a electromagnetic plane wave $A^{\mu}=(0,\vec{A})$ can be calculated analytically by solving the second-order equation

$$\left[\left(\hat{p}-\frac{A}{c}\right)^{2}-c^{2}-\frac{i}{2c}F_{\mu\nu}\sigma^{\mu\nu}\right]\psi=0, \tag{2}$$

and are well known [4]. Here $F_{\mu\nu}=\partial_{\mu}A_{\nu}-\partial_{\nu}A_{\mu}$ is the electromagnetic field tensor and $\sigma^{\mu\nu}=\frac{1}{2}[\gamma^{\mu},\gamma^{\nu}]$. It is convenient to choose the coordinate system in such a way that the electromagnetic field is propagating in the z direction, meaning $\vec{k}=k\hat{e}_{z}$. For a circularly polarized field with $\vec{A}=a_{x}\cos(kx)+a_{y}\sin(kx)=|\vec{A}|[\hat{e}_{x}\cos(kx)+\hat{e}_{y}\sin(kx)]$ the so-called Volkov wave functions [30] are

$$\psi_{q}=\langle\vec{x}|q\rangle=\left[1+\frac{\not{k}\not{A}}{2c(kp)}\right]\frac{u}{\sqrt{2QV}}\times\exp\left[-i(qx)-i\int_{0}^{kx}\frac{(pA)}{c(kp)}d\phi\right], \tag{3}$$

where u represents a bispinor for the free electron which satisfies the first-order Dirac equation without field, and which is normalized by $\overline{uu}=u^{*}\gamma^{0}u=2c^{2}$. The wave functions ψ_{q} are normalized in the volume V. The notation $\not{v}$ for a certain four-vector v^{μ} means the multiplication by the Dirac matrices γ^{μ} while summing over the index μ. The bracket notation (vw) is a short form for the four-scalar product $v^{\mu}w_{\mu}$. The four-vector $q^{\mu}=(Q/c,\vec{q})$ is the label q of the Volkov state $|q\rangle$. Its physical significance is the averaged four-momentum of the particle inside the laser field with wave four-vector k^{μ},

$$q^{\mu}=p^{\mu}-\frac{\overline{A^{2}}}{2(kp)c^{2}}k^{\mu}. \tag{4}$$

Here $\overline{A^{2}}$ denotes the time-averaged square of the four-vector potential of the laser field. The square of this four-vector

$$q^{\mu}q_{\mu}\equiv m_{*}^{2}c^{2} \tag{5}$$

is Lorentz invariant. The parameter m_{*} plays the role of an effective mass of the electron inside the electromagnetic field:

$$m_{*}=\left(1-\frac{\overline{A^{2}}}{c^{4}}\right)^{1/2}. \tag{6}$$

Note that the effective mass becomes larger for increasing vector potential $\vec{A}$, since the Minkowski metric carries a minus sign for the spatial components. Note also that in the case of circular polarization the time average of the square of the vector potential in Eqs. (4) and (6) becomes $\overline{A^{2}}=-|\vec{A}|^{2}=A^{2}$.

In the defining equation (3) for the Volkov states, a physical interpretation can be assigned to the prefactor term in the square bracket acting on the bispinor u. This factor is the remaining part of an exponential term contained in the solution to Eq. (2). All higher orders in k vanish because k is a light four-vector and k and A are transverse: $\not{k}\not{k}=k^{2}=0$ and $(kA)=0$. In fact the second term containing γ matrices in the square bracket in Eq. (3) would be absent in the case of a spinless (Klein-Gordon) particle. It contains information about the spin-dressing field interaction. In other words, the Volkov wave function can be considered as representing the superposition of a free-electron wave (modified by a field-dependent phase), and of a wave generated by the interaction of the spin with the classical single-mode field with vector potential A^{μ}. However, both parts are carry the field-dependent phase, also containing the important contribution of A^{μ}. In fact for an electron Volkov wave this decomposition is rather formal but, as will be shown in the following, it enables the identification of different contributions to the scattering amplitude.

B. Generalized first-Born Mott-scattering cross section

In the lowest-order Born approximation for potential scattering the interaction of the dressed electrons with the central field

$$A^{\mu}_{\mathrm{coul}}=\left(-\frac{Z}{|\vec{x}|},0,0,0\right) \tag{7}$$

is treated as a first-order perturbation. This is well justified if Sommerfeld's fine-structure constant α times the nuclear charge Z is much smaller than the relativistic parameter β according to the condition $Z\alpha\ll\beta=|p|/p_{0}=v/c$ [31]. The transition matrix element for the process $\psi_{i}\rightarrow\psi_{f}$ which needs to be calculated is

$$T_{\mathrm{f}\leftarrow\mathrm{i}}=\frac{iZ}{c}\int d^{4}x\,\overline{\psi_{f}}\frac{\gamma^{0}}{|\vec{x}|}\psi_{i}. \tag{8}$$

This expression corresponds to the process symbolically represented by the diagram in Fig. 1. Here the straight circled lines represent the ingoing and outgoing Volkov electrons. There is an interaction between the electron and the fixed potential denoted by X via the exchange of a virtual photon, represented by a dashed crossed line. The transition amplitude associated with this diagram can be calculated using some generalized Feynman rules, in complete analogy to the free-electron case: It is only necessary in a Feynman-type integral to replace the free-electron wave functions by Volkov wave functions. Though this concept is straightfor-

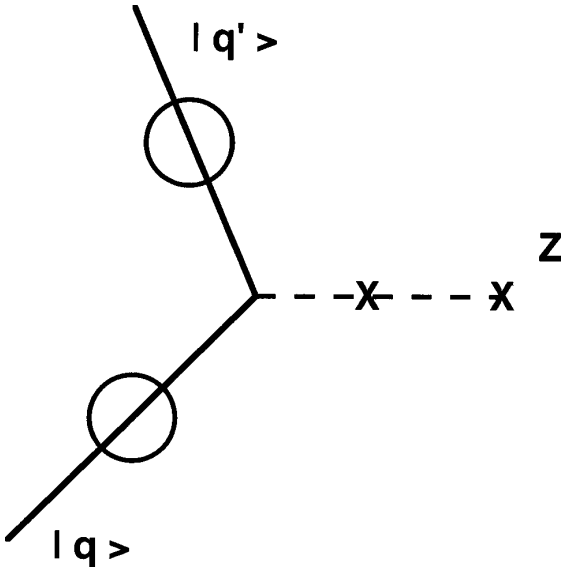

FIG. 1. Feynman diagram describing the elastic potential scattering process of an electron in a Volkov state $|q\rangle$ into a Volkov state $|q'\rangle$ due to the exchange of a virtual photon in the lowest-order (first) Born approximation.

ward, the actual computation is difficult due to the time dependence of Volkov wave functions and also due to the occurrence of a large number of averages over spin-polarized states of the electrons—this leads to the computation of a large amount of traces over products of γ matrices.

Since we are dealing with an intense single-mode laser field, the four-vector potential A^μ does not change appreciably in the collision process. Therefore a Volkov electron in the final state $|q'\rangle$ will have the same invariant effective mass m_*—defined in Eq. (6)—as in the initial state $|q\rangle$. Hence we deduce from Eq. (5) that the averaged four-momenta q^μ and q'^μ must fulfill

$$q^\mu q_\mu = q'^\mu q'_\mu = m_*^2 c^2. \tag{9}$$

Remember that in ordinary Mott scattering the elastic condition $|p|=|p'|$ is obtained using the energy and mass conservation together with the Minkowski scalar product invariance.

Insertion of the Volkov wave functions (3) into Eq. (8) leads to:

$$T_{\mathrm{f\leftarrow i}} = \frac{iZ}{c}\frac{1}{2\sqrt{QQ'V}}\int d^4x\ \overline{u'}\left[1+\frac{\not A \not k}{2c(p'k)}\right]\frac{\gamma^0}{|\vec{x}|}\times\left[1+\frac{\not k \not A}{2c(pk)}\right]u\ \exp\left[-i(q-q')x - i\int_0^{kx}\frac{(pA)}{c(kp)}d\phi + i\int_0^{kx}\frac{(p'A)}{c(kp')}d\phi\right]. \tag{10}$$

The differential cross section $d\sigma$ for the scattering process represented by the diagram in Fig. 1 is proportional to the square of $T_{f\leftarrow i}$, to the density of final states $|q'\rangle$ in phase space divided by time T and to the incoming flux of electrons:

$$d\sigma = \frac{|T_{f\leftarrow i}|^2}{T}\left(\frac{Vd^3q'}{8\pi^3}\right)\frac{QV}{c^2|\vec{q}|}. \tag{11}$$

Using Eq. (10) for $T_{f\leftarrow i}$, the following expression is obtained:

$$d\sigma = \frac{Z^2}{c^2}\left|\int d^4x\ \overline{u'}\left[1+\frac{\not A \not k}{2c(p'k)}\right]\frac{\gamma^0}{|\vec{x}|}\left[1+\frac{\not k \not A}{2c(pk)}\right]u \times\exp\left[-i(q-q')x - i\int_0^{kx}\frac{(pA)}{c(kp)}\,d\phi + i\int_0^{kx}\frac{(p'A)}{c(kp')}d\phi\right]\right|^2\frac{d^3q'}{32\pi^3Q'c^2|\vec{q}|T}. \tag{12}$$

Using the abbreviation

$$\alpha_i = \frac{1}{c}\left(\frac{pA_i}{kp} - \frac{p'A_i}{kp'}\right), \tag{13}$$

where $i\in\{x,y\}$, the occurring time dependence in the exponent can be rewritten as

$$-i\alpha_x\sin(kx) + i\alpha_y\cos(kx) \equiv -i\zeta\ \sin(kx-\phi_0), \tag{14}$$

where the new amplitude ζ is

$$\zeta = \frac{1}{c}\left(\left[\frac{pA_x}{(kp)} - \frac{p'A_x}{(kp')}\right]^2 + \left[\frac{pA_y}{(kp)} - \frac{p'A_y}{(kp')}\right]^2\right)^{1/2}, \tag{15}$$

and the associated phase ϕ_0 reads

$$\phi_0 = \arccos\left[\frac{1}{c\zeta}\left(\frac{pA_x}{kp} - \frac{p'A_x}{kp'}\right)\right]. \tag{16}$$

The three different time dependences in Eq. (12) can be transformed by well-known identities involving ordinary Bessel functions J_n:

$$\left\{\begin{array}{c}1\\ \cos(kx)\\ \sin(kx)\end{array}\right\}\times\exp[-i\zeta\ \sin(kx-\phi_0)] = \sum_n\ \exp(-inkx) \times\left\{\begin{array}{c} J_n(\zeta)e^{(in\phi_0)}\\ \frac{1}{2}\{J_{n+1}(\zeta)e^{[i(n+1)\phi_0]} + J_{n-1}(\zeta)e^{[i(n-1)\phi_0]}\}\\ \frac{1}{2i}\{J_{n+1}(\zeta)e^{[i(n+1)\phi_0]} - J_{n-1}(\zeta)e^{[i(n-1)\phi_0]}\}\end{array}\right\} \equiv \sum_n\ e^{(-inkx)}\times\left\{\begin{array}{c}B_n(\zeta,\phi_0)\\ Bc_n(\zeta,\phi_0)\\ Bs_n(\zeta,\phi_0)\end{array}\right\}. \tag{17}$$

Using these transformations in Eq. (12), we obtain the following expression for the differential cross section $d\sigma$:

$$d\sigma=\frac{Z^2}{c^2}\left|\sum_{n=-\infty}^{\infty}\int d^4x[\overline{u'}\gamma^0 u]B_n\frac{\exp[-i(q-q'+nk)x]}{|\vec{x}|}+\int d^4x\left\{\left[\overline{u'}\frac{\not{A}_x\not{k}}{2c(kp')}\gamma^0 u+\overline{u'}\gamma^0\frac{\not{k}\not{A}_x}{2c(kp)}u\right]Bc_n\right.$$
$$+\left[\overline{u'}\frac{\not{A}_y\not{k}}{2c(kp')}\gamma^0 u+\overline{u'}\gamma^0\frac{\not{k}\not{A}_y}{2c(kp)}u\right]Bs_n$$
$$\left.+\frac{-A^2}{4c^2(kp)(kp')}[\overline{u'}\not{k}\gamma^0\not{k}u]B_n\right\}\frac{\exp[-i(q-q'+nk)x]}{|\vec{x}|}\Bigg|^2\frac{d^3q'}{32\pi^3Q'c^2|\vec{q}|T}. \tag{18}$$

We wish to emphazise again that the influence of the field is completely taken care of. However, due to the fact that the Volkov wave functions contain two components, there are four different amplitudes interfering during the scattering process. The remaining integrals can be reduced using the well-known identity

$$\int d^4x\frac{\exp[-i(q-q'+nk)x]}{|\vec{x}|}=\frac{8\pi^2c\,\delta(Q-Q'+n\omega)}{|\vec{q}-\vec{q}'+n\vec{k}|^2}. \tag{19}$$

Hence the differential cross section can be written

$$d\sigma=\frac{Z^2}{c^2}\left|\sum_{n=-\infty}^{\infty}\left[(\overline{u'}\gamma^0 u)B_n+\left(\overline{u'}\frac{\not{A}_x\not{k}}{2c(kp')}\gamma^0 u+\overline{u'}\gamma^0\frac{\not{k}\not{A}_x}{2c(kp)}u\right)Bc_n+\left(\overline{u'}\frac{\not{A}_y\not{k}}{2c(kp')}\gamma^0 u+\overline{u'}\gamma^0\frac{\not{k}\not{A}_y}{2c(kp)}u\right)Bs_n\right.\right.$$
$$\left.\left.-\frac{A^2}{4c^2(kp)(kp')}(\overline{u'}\not{k}\gamma^0\not{k}u)B_n\right]\frac{2\pi\delta(Q-Q'+n\omega)}{|\vec{q}-\vec{q}'+n\vec{k}|^2}\right|^2\frac{d^3q'}{2\pi Q'|q|T}, \tag{20}$$

where $A_x=(0,|\vec{A}|,0,0)$ and $A_y=(0,0,|\vec{A}|,0)$. The appropriate expression for the square of the δ function occurring in this formula is obtained by the usual procedure [31]. This leads to the expression

$$d\sigma=\frac{Z^2}{c^2}\sum_{n=-\infty}^{\infty}\left|[\overline{u'}\gamma^0 u]B_n+\left[\overline{u'}\frac{\not{A}_x\not{k}}{2c(kp')}\gamma^0 u+\overline{u'}\gamma^0\frac{\not{k}\not{A}_x}{2c(kp)}u\right]Bc_n+\left[\overline{u'}\frac{\not{A}_y\not{k}}{2c(kp')}\gamma^0 u+\overline{u'}\gamma^0\frac{\not{k}\not{A}_y}{2c(kp)}u\right]Bs_n\right.$$
$$\left.-\frac{A^2}{4c^2(kp)(kp')}[\overline{u'}\not{k}\gamma^0\not{k}u]B_n\right|^2\frac{\delta(Q-Q'+n\omega)}{|\vec{q}-\vec{q}'+n\vec{k}|^4}\times\frac{d^3q'}{Q'|\vec{q}|}. \tag{21}$$

The calculation is now reduced to the computation of the products containing γ matrices. For unpolarized electrons the averaging procedure can be performed using the trace technique. Details of the actual calculation can be found in the Appendix.

C. Final expression

The differential cross section can ultimately be expressed in terms of only the averaged momenta $\vec{q}$ and $\vec{q}'$: Using the abbreviation $\tilde{v}^\mu=(v^0,-\vec{v}^i)$, we note that

$$(kq)=k^\mu p_\mu-\frac{\overline{A^2}}{2(kp)c^2}k^\mu k_\mu=(kp),$$

$$(k\tilde{q})=k^\mu\tilde{p}_\mu-\frac{\overline{A^2}}{2(kp)c^2}k^\mu\tilde{k}_\mu=(k\tilde{p})-\frac{\overline{A^2}\omega^2}{(kp)c^4}, \tag{22}$$

and $(Aq)=(Ap)$. It turns out to be convenient to define

$$\mathring{A}\equiv(0,\,a_x\cos\phi_0,a_y\sin\phi_0,0) \tag{23}$$

in order to write the cross section in a more compact form. The volume element d^3q' in momentum space can be transformed according to $d^3q'=|\vec{q}'|Q'/c^2dQ'do$. Here o denotes the solid angle. The δ function arising from integral (19) expresses the energy conservation in the multiphoton processes that occur. This leads to the final expression

$$\frac{d\sigma}{do}=\sum_n \left.\frac{d\sigma^{(n)}}{do}\right|_{Q'=Q+n\omega}. \tag{24}$$

In addition, using condition (9), it follows that the final quasimomentum reads

$$|\vec{q}'|=\left(|\vec{q}|^2+2n\,\frac{\omega Q}{c^2}+\frac{n^2\omega^2}{c^2}\right)^{1/2} \tag{25}$$

for a process involving n photons. In the nonrelativistic limit, this expression in fact reaches the well-known condition $|\vec{p}'|=\sqrt{2E+2n\omega}$. The differential cross section $d\sigma^{(n)}/do$ for each scattering process, resulting in the net exchange of n photons, is

$$\begin{aligned}\frac{d\sigma^{(n)}}{do}=&\frac{Z^2|\vec{q}'|}{c^2|\vec{q}|}\frac{1}{|\vec{q}-\vec{q}'+n\vec{k}|^4}\Bigg[2J_n(\zeta)^2\Bigg\{\left[c^2+\frac{QQ'}{c^2}+\vec{q}\vec{q}'+\frac{A^2}{2c^2}\left(\frac{(k\tilde{q}')}{(kq)}+\frac{(k\tilde{q})}{(kq')}\right)+\frac{(A^2)^2\omega^2}{2c^6(kq)(kq')}\right]\left(1-\frac{A^2\omega^2}{c^4(kq)(kq')}\right)\\&-\frac{A^2}{2c^2}\left[1-\frac{(k\tilde{q}')(k\tilde{q})}{(kq)(kq')}\right]+\frac{(A^2)^2\omega^2}{c^6(kq)(kq')}+\frac{(A^2)^2\omega^2}{2c^6(kq)^2(kq')^2}\left[(kq')(k\tilde{q}')+(kq)(k\tilde{q})+\frac{A^2\omega^2}{c^4}\right]\Bigg\}\\&+[J_{n+1}(\zeta)^2+J_{n-1}(\zeta)^2]\Bigg\{\frac{-A^2}{2c^2}\left[\frac{(k\tilde{q}')}{(kq)}+\frac{(k\tilde{q})}{(kq')}+1+\frac{(k\tilde{q})(k\tilde{q}')-2\omega^2}{(kq)(kq')}+\frac{2A^2\omega^2}{c^4(kq)(kq')}+\frac{A^2\omega^2}{c^4(kq)(kq')}\right.\\&\left.\times\left((kq')(k\tilde{q}')+(kq)(k\tilde{q})+\frac{A^2\omega^2}{c^4}\right)-\frac{2\omega^2}{c^2(kq)(kq')}\left(\frac{QQ'}{c^2}+\vec{q}\vec{q}'+\frac{A^2}{2c^2}\left(\frac{(k\tilde{q}')}{(kq)}+\frac{(k\tilde{q})}{(kq')}\right)+\frac{(A^2)^2\omega^2}{2c^6(kq)(kq')}\right)\right]\\&+\frac{2A^2\omega^2}{c^4(kq')(kq)}[q_x'q_x+q_y'q_y]\Bigg\}+J_{n+1}(\zeta)J_{n-1}(\zeta)\cos(2\phi_0)\,\frac{2A^2\omega^2}{c^4(kq')(kq)}[q_x'q_x-q_y'q_y]+J_n(\zeta)[J_{n+1}(\zeta)+J_{n-1}(\zeta)]\\&\times\Bigg\{-\frac{2A^2\omega^2}{c^4(kq)(kq')}\left[\frac{(\mathring{A}q)}{c}+\frac{(\mathring{A}q')}{c}\right]+\frac{(\mathring{A}q')(k\tilde{q})}{c(kq')}+\frac{(\mathring{A}q)}{c}+\frac{(\mathring{A}q')}{c}+\frac{(\mathring{A}q)(k\tilde{q}')}{c(kq)}\Bigg\}\Bigg]\Bigg|_{Q'=Q+n\omega}.\end{aligned} \tag{26}$$

This formula is a relativistic generalization of the Bunkin and Fedorov treatment [13], and it represents a specialization for circular polarization of the general expression of Denisov and Fedorov [19].

By inspection of Eq. (26) we note two features. On the one hand, the laser field A enters this expression in an intricate way, not only through the arguments of the Bessel functions, it is also present in multiplicative factors in front of the squares of Bessel functions. On the other hand, several additional terms arise from the averaging calculation over spin polarizations.

When no laser field is present, the additional spin sums in Eq. (26) vanish, while all Bessel functions vanish except for $n=0$: It is $J_n(0)=\delta_{n0}$. In this case the result reduces, after integration over the final energy variable, to the well-known unpolarized Mott cross section for potential scattering,

$$\frac{d\sigma}{do}=\frac{1}{4}\frac{Z^2\alpha^2}{|\vec{p}|^2\beta^2}\frac{1-\beta^2\sin^2(\theta/2)}{\sin^4(\theta/2)}, \tag{27}$$

where $\theta=\angle(\vec{p},\vec{p}')$; see, for instance, Bjorken and Drell or Itzykson and Zuber [32].

III. SIMPLIFIED TREATMENTS

A. Comparison to the scattering of a spinless particle

We now briefly consider an analogous calculation for obtaining the differential cross section for a spinless particle. Its wave function will obey the Klein-Gordon equation for bosons with spin zero, which is in fact the second-order equation (2) without the term $-i/2cF_{\mu\nu}\sigma^{\mu\nu}$. The corresponding Volkov solutions can be found analogously to the described treatment for electrons, and in this case read

$$\psi_q=\langle\vec{x}|q\rangle=\left(\frac{c}{2QV}\right)^{1/2}\exp\left[-i(qx)-i\int_0^{kx}\frac{(pA)}{c(kp)}d\phi\right]. \tag{28}$$

Note that they do not contain the square bracket prefactor acting on a bispinor which is a feature of the fermion character of electrons in Eq. (3).

The transition matrix element $T_{f\leftarrow i}$ involved in the calculation of the Coulomb scattering does not exhibit the spin effects appearing for electrons. The expression to be calculated is

$$T_{f\leftarrow i}=\frac{i}{c}\int d^4x\,\psi_f^*(p_\mu A^\mu_{\rm coul}+A^\mu_{\rm coul}p_\mu)\psi_i\,. \tag{29}$$

There is no spin-averaging procedure here. Consequently, the trace to be evaluated in the case of a fermion, which leads in the limit of vanishing vector potential to the Mott factor, does not occur. Finally, the energy dependence of the cross section is again a comb of δ-functions and the n-photon cross sections read

$$\begin{aligned}\frac{d\sigma^{(n)}}{do}=&\frac{Z^2|\vec{q}\,'|}{c^4|\vec{q}|}\frac{1}{|\vec{q}-\vec{q}\,'+n\vec{k}|^4}\Bigg(J_n(\zeta)^2(Q'+Q)^2+J_n(\zeta)[J_{n+1}(\zeta)+J_{n-1}(\zeta)]\omega(Q'+Q)[(\zeta_f\cos\phi_f+\zeta_i\cos\phi_i)\cos(\phi_0)\\&+(\zeta_f\sin\phi_f+\zeta_i\sin\phi_i)\sin(\phi_0)]+\tfrac{1}{2}J_{n-1}(\zeta)J_{n+1}(\zeta)\sin(2\phi_0)[\zeta_f\cos\phi_f+\zeta_i\cos\phi_i][\zeta_f\sin\phi_f+\zeta_i\sin\phi_i]\\&+\frac{\omega^2}{4}[J_{n+1}(\zeta)^2+J_{n-1}(\zeta)^2][(\zeta_f\cos\phi_f+\zeta_i\cos\phi_i)^2+(\zeta_f\sin\phi_f+\zeta_i\sin\phi_i)^2]\\&+\frac{\omega^2}{2}J_{n+1}(\zeta)J_{n-1}(\zeta)\cos(2\phi_0)[(\zeta_f\cos\phi_f+\zeta_i\cos\phi_i)^2-(\zeta_f\sin\phi_f+\zeta_i\sin\phi_i)^2]\Bigg)\Bigg|_{Q'=Q+n\omega},\end{aligned} \tag{30}$$

where ζ_j and ϕ_j with $j\in\{i,f\}$ denote the corresponding definitions of amplitude (15) and phase (16) for initial and final states, respectively. In the case when no laser field is present, this expression reduces, after integration over the final energy variable, to the spinless meson cross section

$$\frac{d\sigma}{do}=\frac{1}{4}\frac{Z^2\alpha^2}{|\vec{p}|^2\beta^2\sin^4(\theta/2)}, \tag{31}$$

where $\theta=\angle(\vec{p},\vec{p}\,')$; see again Ref. [32].

B. Comparison to the nonrelativistic expression

In order to compare our findings to a nonrelativistic treatment, one should note that the terms in the outer large normal brackets in expression (26) arise from the spin-averaging procedure. In fact the analogous calculation for a spinless particle leading to Eq. (30) has to be used for discussing the nonrelativistic limit.

The nonrelativistic transition matrix element

$$T_{f\leftarrow i}=-i\int_{-\infty}^{\infty}d\tau\langle\vec{p}_f(\tau)|\frac{-Z}{r}|\vec{p}_i(\tau)\rangle \tag{32}$$

has to be calculated, where $|\vec{p}\rangle$ are nonrelativistic Volkov states. In position space, for the case of circular polarized radiation in the Coulomb gauge $\vec{\nabla}\cdot\vec{A}=0$, they read

$$\langle\vec{x}|\vec{p}(\tau)\rangle=\left(\frac{1}{V}\right)^{1/2}\exp\left\{-\frac{i}{2}\int^{\tau}dt\left[\vec{p}-\frac{\vec{A}(\vec{x},t)}{c}\right]^2\right\}\exp(i\vec{p}\cdot\vec{r}), \tag{33}$$

normalized in the volume element V. An analogous transformation of the integral in Eq. (32) leads to ordinary Bessel functions J_n. Note that in this case the additional term in the averaged momentum of Eq. (4) becomes independent of the orientation of the momentum vector. Hence for the differential cross section the nonrelativistic limit of Eq. (26) without spin terms is obtained:

$$\frac{d\sigma^{(n)}}{do}=\frac{4Z^2|\vec{q}\,'|}{c^4|\vec{q}|}J_n^2\left(\frac{|A|}{c\omega}|\vec{p}-\vec{p}\,'|\right)\frac{c^4}{|\vec{p}-\vec{p}\,'+n\vec{k}|^4}\Bigg|_{E'=E+n\omega}. \tag{34}$$

The modulus of the final momentum $|\vec{p}\,'|$ is fixed due to energy conservation: $|\vec{p}\,'|=\sqrt{2(E+n\omega)}$. In comparison to Eq. (30) we observe two features. On the one hand, the arguments of the Bessel functions here are the nonrelativistic limit of ζ defined above, since the four-vector product (kp) has in atomic units the nonrelativistic limit ω. On the other hand, for nonrelativistic intensities, the terms proportional to the vector potential $\vec{A}$ can be neglected and we have $(Q+Q')^2\simeq 4c^4$. Then expression (30) for a spinless particle reduces to the nonrelativistic result.

IV. INFLUENCE OF SPIN-ORBIT AND SPIN-LASER INTERACTIONS

A. Kinematics of the collision

We turn now to a qualitative and quantitative discussion of the main features of the differential cross section (26) in close comparison to the spinless and nonrelativistic expressions. For this purpose a coordinate system in which $\vec{k}\|\hat{e}_z$ for the description of the scattering geometry is introduced as shown in Fig. 2.

In this system $\vec{q}\in\mathrm{span}(\hat{e}_z,\hat{e}_x)$. The angles between the averaged momentum vectors and the field propagation vector are $\psi=\angle(\vec{q},\vec{k})$, $\vartheta=\angle(\vec{k},\vec{q}\,')$, and $\varphi=\angle(\vec{q}_\perp,\vec{q}\,'_\perp)$, meaning that ϑ and φ denote the usual angular variables in spheri-

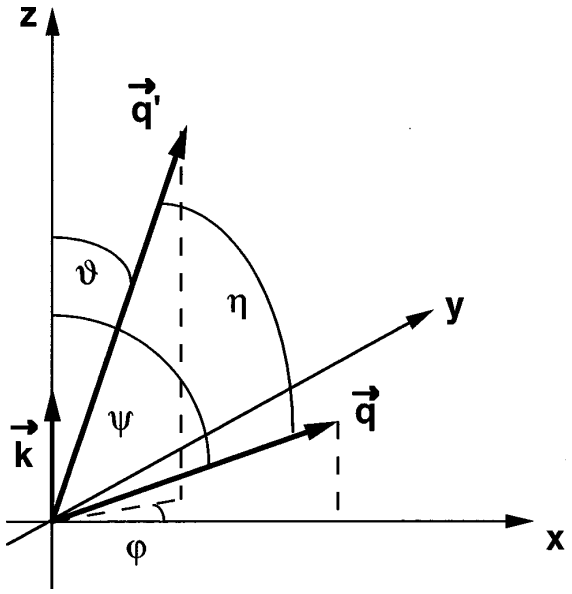

FIG. 2. Coordinate system used in the description of the scattering processes. For a definition of the variables used, see the text.

cal coordinates for $\vec{q}'$. The cosine of the angle η between $\vec{q}$ and $\vec{q}'$ can be calculated by some simple trigonometric relations.

Choosing these angles for a given direction of observation depending on energy and momentum of the incoming electrons depending on the experimental conditions, the energy distribution of the scattered electrons is obtained as a parametric function. For the sake of illustration, the following angles have been chosen: $\psi=\pi/2$, $\varphi=\pi/2$, and $\vartheta=\pi/2$, meaning $\vec{q}\|\hat{e}_x$ and $\vec{q}'\|\hat{e}_y$. We investigated a range of other parameters but did not find a significant change of qualitative behavior, although there are quantitative differences. Regarding the incoming projectile, the parameters which have to be chosen are, on the one hand, the initial kinetic energy

$$W_{\mathrm{kin}}=c^2(\gamma-1), \tag{35}$$

where $\gamma=1/\sqrt{1-\beta^2}=1/\sqrt{1-v^2/c^2}$ is the relativistic parameter, and, on the other hand, the component of the initial average electron momentum $\vec{q}$ parallel to the field propagation direction $\vec{k}$. This choice fixes all other quantities involved using Eqs. (4) and (6). As a typical near-infrared laser angular frequency we have chosen the one of a neodymium laser: $\omega=0.043$ a.u., for all numerical evaluations.

B. Nonrelativistic regime

In the limit of slow electron velocities and moderate field strengths the effects of the additional spin terms and the dependence of q^μ on the spatial orientation of the electron momentum due to (kp) are expected to be small. In this case the final expression (26) can be compared to the corresponding expression for a spinless particle, Eq. (30), and to the Bunkin-Fedorov nonrelativistic treatment, Eq. (34). As an example we chose the electron kinetic energy to be $W_{\mathrm{kin}}=100$ a.u.$\simeq 2.7$ keV, and the z component of the momentum $\vec{q}$ to be $q_z=0$.

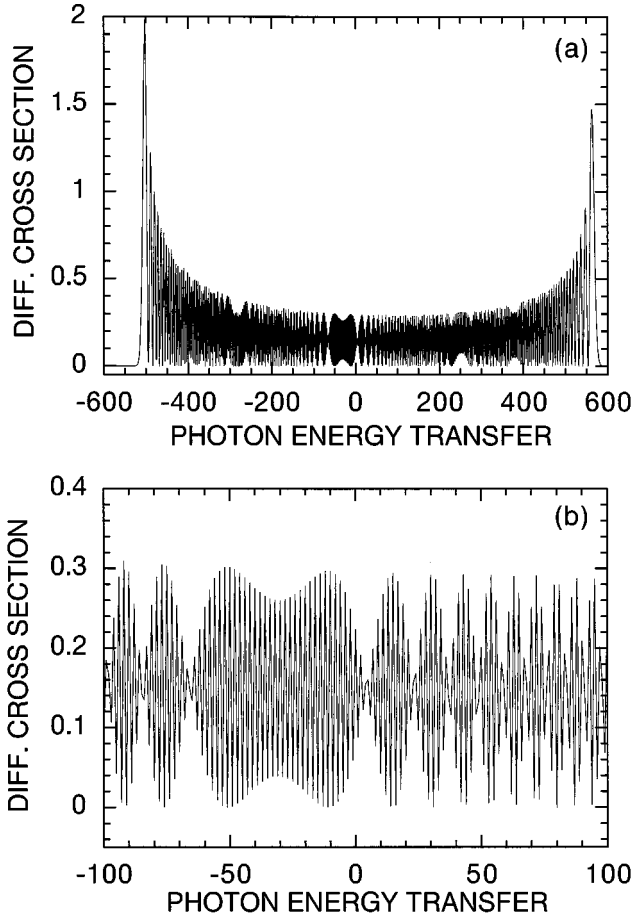

FIG. 3. Envelope of the differential cross section $d\sigma/do$ scaled in 10^{-7} a.u. as a function of energy transfer $Q'-Q$ scaled in units of the laser photon energy ω for an electrical field strength of $E=0.05$ a.u. or a vector potential $A=159.3$ a.u. The initial electron energy is $W=100$ a.u. The expressions for spinless particles and for the nonrelativistic case give visibly identical spectra. The upper picture (a) shows the complete final-energy spectrum. In the lower picture (b), a magnification of the central part around the elastic peak is shown.

For an electrical field strength of $E=0.05$ a.u. corresponding to a moderate intensity of $I=8.75\times10^{13}$ W/cm^2, the differential cross section given by the generalized equation (26) is plotted in the upper part (a) of Fig. 3 as a function of the final electron energy scaled to the photon energy. The scattering angle has been chosen to be large enough, corresponding to a large momentum transfer, so that significant numbers of photons can be exchanged in the course of the collision. In this relatively low-intensity regime, no difference can be seen between the various treatments discussed here, i.e., the cross section as computed from the full treatment, Eq. (26), the one obtained from Eq. (30) derived for a spinless particle, and the one predicted by the nonrelativistic treatment according to Eq. (34). One observes that for this collision geometry, a set of up to several hundred photons can be exchanged, in spite of the moderate laser intensity. The heights of the different photon-energy-transfer peaks depend crucially on the values of the ordinary Bessel functions. The spectrum exhibits an overall asymmetric envelope for peaks of negative energy transfer, higher than peaks for positive energy transfer. Also, there is an asymmetry of the spec-

trum in the sense that it is more extended on the absorption side (positive energy transfer) than on the emission side (negative energy transfer). For this choice of parameters the observed cutoffs are found to be at about $+570\omega$ and -500ω, respectively. Note that in the case of stimulated emission the final energy of the electron is still around 2.2 keV. Though the kinetic energies of the scattered electrons are remarkably redistributed over more than 1 keV, no net overall heating or cooling effect occurs. In fact, we checked that the average value of the kinetic-energy transfer is almost zero. Around the central elastic peak at zero an oscillatory behavior is found which is magnified in the lower part (b) of Fig. 3. There is a slight, but notable shift of -30ω of a nearly mirror-symmetry axis for the occurring oscillations. The magnitude of the shift depends on the choice of the angular parameters, as explained below.

An investigation of other choices for the kinematical parameters reveals qualitatively the same behavior, though of course quantitative modifications occur. Then the origin of the asymmetry in the distribution can be traced back to the dependence of the modulus of the final momentum $|\vec{q}'|$ on the photon-energy-transfer number n according to Eq. (25). In the denominator $|\vec{q}-\vec{q}'+n\vec{k}|^4$ of Eqs. (26) and (30), the term $\vec{q}'\cdot\vec{q}'$ makes a contribution $2n\omega Q/c^2$, which accounts for most of the asymmetry envelope. Depending on the sign of n this term makes the denominator increase in the case $n<0$, and decrease in the case $n>0$, yielding an enhancement of negative over positive-energy-transfer cross sections. At the same time, the positions of the maxima at the edges of the energy distributions are determined by the magnitude of the argument ζ of the Bessel functions and can be found for photon energy transfers when the order of the function roughly equals its argument. In this case, the Bessel function J_n can be expressed in terms of the Airy function Ai according to [33]

$$J_n(n+zn^{1/3})\simeq 2^{1/3}n^{-1/3}\mathrm{Ai}(-2^{1/3}z), \tag{36}$$

which reaches its maximum value near $z=0$. This implies as well that the positions of the edges of the distribution depend on the momentum transfer and consequently on the scattering angle. In addition, ζ is slightly dependent on n, which amplifies the asymmetry between the positions of the two edges. In addition, for increasing order n and fixed argument, the value of J_n is decreasing with n^{-n}, when $n\gg|\zeta|$. This explains why the cross section falls off abruptly beyond the points where the argument of the Bessel functions equal to the order.

Concerning the extension of the structure, the maximum transfer of energy between the field and the projectile during the scattering can be explained in a simple manner using either the classical or quantum pictures. In fact, the argument ζ of the Bessel functions is in some sense a measure for the difference of the transient change in energy between the incoming and outgoing dressed electrons. This is most clearly seen in the nonrelativistic limit.

In the classical picture, the time-dependent energy of the electron contains, in addition to the mean value, a time-dependent contribution

$$W(t)=\frac{p^2}{2}+\frac{E^2}{2\omega^2}+\frac{\vec{E}\cdot\vec{p}}{\omega}=W_{\mathrm{kin}}+W_{\mathrm{osc}}+W_{\mathrm{trans}}(t). \tag{37}$$

Depending on the phase of the field, the incoming electron actually has gained or lost a certain amount of energy on its way through the field when it collides elastically with the nucleus, thereby changing its propagation direction but leaving the actually acquired energy unchanged. Therefore, the collision process transforms transient oscillatory energy into real changes of kinetic energy of the electron. The transient energy difference scaled to the photon energy then reads

$$\begin{aligned}(W_{\mathrm{trans}}-W'_{\mathrm{trans}})/\omega&=\vec{E}\cdot(\vec{p}-\vec{p}')/\omega^2\\&=\frac{E}{\omega^2}|\vec{p}-\vec{p}'|\cos[\angle(\vec{E},\vec{p}-\vec{p}')].\end{aligned} \tag{38}$$

For a given scattering geometry the angle is phase dependent, and extremal energy transfer is obtained when the cosine equals ± 1. For the present kinematics this scaled maximal transient energy difference is 540. The interesting point is that this quantity is in fact the argument $\zeta=E|\vec{p}-\vec{p}'|/\omega^2$ of the Bessel functions entering expression (34), which results from the nonrelativistic quantum calculation. Hence the difference of the maximal variation of the energy corresponds to the range of the peak structure in the laser-assisted cross section, meaning the maximal change in final mean energy.

C. Relativistic regime and spin effects

The major effect of increasing the field strength is to increase considerably the maximum number of photons exchanged, although the overall shape of the energy distribution of the scattered electrons is globally similar to the one displayed in upper part (a) of Fig. 3. For example, when increasing the field strength to $E=1$ a.u., corresponding to an intensity of about 3.5×10^{16} W/cm^2, while keeping the same electron velocity such as $W_{\mathrm{kin}}=100$ a.u.$\simeq 2.7$ keV. Then up to about 27 000 photons can be absorbed, as shown in Fig. 4, where the absorption edge structure is shown. Note the change of scale. The solid line denotes the result according to the full treatment, Eq. (26), the short dashed line sketches the result according to Eq. (30) for a spinless particle, while the long dashed line gives the result of the nonrelativistic calculation according to Eq. (34). While there is only a minor difference between the two relativistic calculations, there is a notable shift of about 200 photon energies less in the nonrelativistic treatment. We conclude from these findings that relativistic mass shift effects show up in this regime of intensities attainable with currently operated laser sources. In particular, for a given electron momentum $\vec{p}$, the nonrelativistic limit $(kp)\rightarrow\omega$ can no longer be performed for the determination of the average momentum $\vec{q}$, which is of crucial importance inside the argument ζ of the Bessel functions. Nevertheless, almost no spin effects occur.

Note that we have not shown the central part of the distribution which corresponds to moderate photon energy

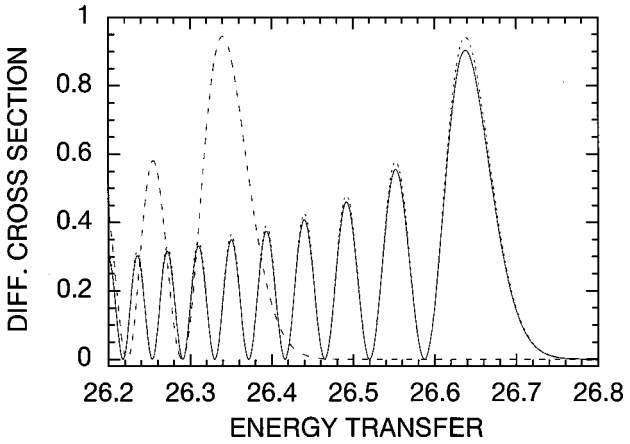

FIG. 4. Envelope of the absorption edge part of the differential cross section $d\sigma/do$ scaled in 10^{-9} a.u. as a function of energy transfer $Q'-Q$ scaled in units of 1000ω for an electrical field strength of $E=1$ a.u. or a vector potential $A=3186$ a.u. The initial electron energy is $W=100$ a.u. The solid line denotes the result for electrons, the short dashed one the differential cross section for spinless particles, and the long dashed one the result for the nonrelativistic limit.

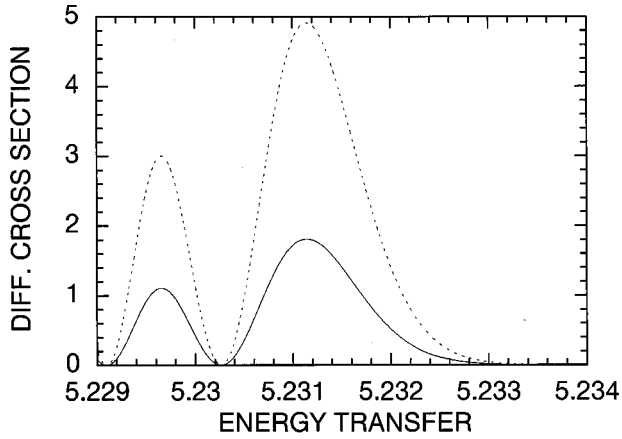

FIG. 5. Envelope of the absorption edge part of the differential cross section $d\sigma/do$ scaled in 10^{-14} a.u. as a function of energy transfer $Q'-Q$ scaled in units of $10^5\omega$ for an electrical field strength of $E=5.89$ a.u. or a vector potential $A=18\,769$ a.u. The initial electron energy is $W=c^2$. The solid line denotes the result for electrons, and the dashed line sketches the result for spinless particles.

transfers. Its overall envelope exhibits regular oscillations in the peak height. In this regime, the argument ζ of the Bessel function is much larger than the order n. The principal asymptotic form of ordinary Bessel functions $J_n(\zeta)$ are well known: Under the condition $8\zeta \gg 4n^2-1$ the asymptotic expression is

$$J_n(\zeta) \simeq \left(\frac{2}{\pi\zeta}\right)^{1/2} \cos\left[\zeta-(n+1/2)\frac{\pi}{2}\right], \tag{39}$$

where n is fixed, and ζ becomes large [33]. Therefore we conclude that in strong fields the Bessel functions for moderate energy transfer can be replaced by periodic cosine functions. Since ζ depends in first order linearly on the exchanged photon momentum $n\omega$, the variations of the cross section reveal several oscillating envelopes for the different momentum transfers. The number of oscillations depends on the direction of observation, because ζ depends on it as well.

As a typical example of relativistic regime, the electrical field strength of $E=5.89$ a.u. corresponding to about 1.2×10^{18} W/cm^2 and $W_{\rm kin}=c^2$ or $\gamma=2$ is considered. Note that in such a high field the initial condition $\psi=\pi/2$ can no longer be fulfilled for a relatively slow electron with $W_{\rm kin}=100$ a.u. because of the important radiation pressure in the $\vec{k}$ direction. In order to keep the same illustrative choice of angles, the kinetic energy of the electron has to be increased. Now, significant differences occur at the absorption edge, which lies at about 523100 photon energies. In Fig. 5 the solid line denotes the differential cross section according to expression (26) for the Dirac electron, and the dashed line sketches the result for spinless particles from Eq. (30). Since in both cases the same argument ζ occurs in the Bessel function, the cutoff is found at the same position. Nevertheless, the cross section for electrons is smaller by a factor of 3. Here the difference between the spinless and exact Dirac treatments is of the same order of magnitude as the one observed for the Mott scattering itself, namely, in the absence of the laser field. This clearly indicates that it is the contribution associated to the free bispinor part of the Volkov wave function which dominates the cross section: the Mott factor due to spin-orbit coupling reduces large angle scattering.

D. Angular distributions: Mott effect and light pressure

As was shown above, for strong fields the central part of the spectrum consists of peaks whose heights are determined by oscillations in the values of the Bessel function. Since, compared to the electron kinetic energy, the photon energy is small, those details of the spectrum might not be of interest, but instead several lines inside a detection window will be observed. For this reason ±100 peaks around the elastic one were summed in order to draw the angular dependence of the $\eta=\pi/2$ scattering.

In Fig. 6 the accumulated differential cross section is shown for an electrical field strength of $E=1$ a.u. and a kinetic energy of $W_{\rm kin}=100$ a.u. as functions of angle ϑ in degrees. Apart from the minor differences in the magnitudes all three calculations exhibit maxima for $\vartheta=0°$ and 180° a smooth oscillatory behavior, the minima in the nonrelativistic calculation at $\vartheta=-90°$ and 90°, while they are slightly shifted in both relativistic calculations.

This trend is even more pronounced for the kinetic energy $W_{\rm kin}=c^2$ a.u., as can be seen in Fig. 7. While the nonrelativistic treatment (long dashed line) again predicts the oscillatory behavior, both relativistic calculations lead to peaked structures in the direction of the laser propagation $\vartheta=0°$. The Volkov electron cross section (solid line) is below the spinless particle result (short dashed line). It is reduced due to the Mott factor governing the dominant contribution from the free bispinor part of the Volkov wave function.

For the relativistic field strength of $E=5.89$ a.u. and the kinetic energy of $W_{\rm kin}=4c^2$ a.u., the accumulated differential cross section is plotted in Fig. 8. Here again the thick solid line denotes the result for the Volkov electron, the short dashed line the spinless particle, and the long dashed line the

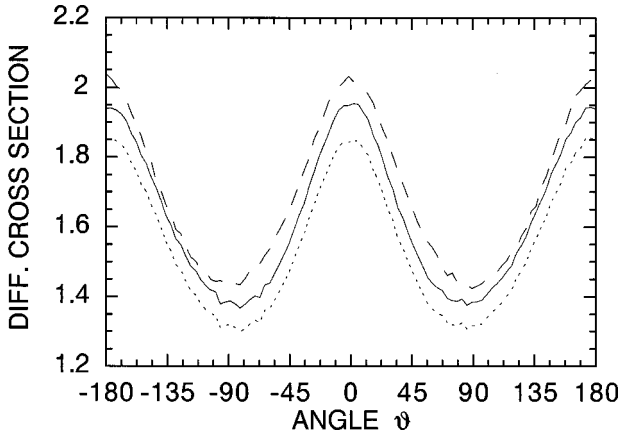

FIG. 6. Summed differential cross sections $d\sigma/do$ scaled in 10^{-7} a.u. of ± 100 peaks around the elastic one as a function of the angle ϑ for an electrical field strength of $E=0.05$ a.u. The electron energy is $W=100$ a.u.$\simeq 2.7$ keV. The relativistic parameter is $\gamma \simeq 1.0053$. The solid line denotes the result for electrons, the short dashed one sketches the values for spinless particles, and the long dashed one is the result for the nonrelativistic limit.

nonrelativistic values. While the difference from the nonrelativistic result is even larger, now it is found that the Volkov electron cross section is larger than the one for the spinless particle around the direction of $\vec{k}$ at $\vartheta=0°$.

In Fig. 8 the contribution of the free bispinor part of the Volkov wave function is plotted as the thin solid line in comparison to the Volkov electron (solid) and spinless particle (long dashed) results. This contribution, governed by the Mott factor, is still always smaller than the cross section for spinless particles. These considerations show clearly that in this ultrahigh-field strength regime stimulated processes become important, and lead to momentum transfer in the direction of propagation of the electromagnetic field.

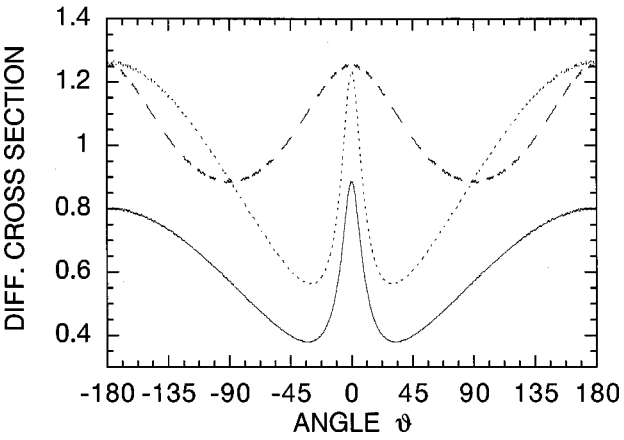

FIG. 7. Summed differential cross sections $d\sigma/do$ scaled in 10^{-12} a.u. of ± 100 peaks around the elastic one as a function of the angle ϑ for an electrical field strength of $E=1$ a.u. The electron energy is $W=c^2=137^2$ a.u., and the relativictic parameter is $\gamma=2$. The solid line denotes the result for electrons, the short dashed one sketches the values for spinless particles, and the long dashed one is the result for the nonrelativistic limit.

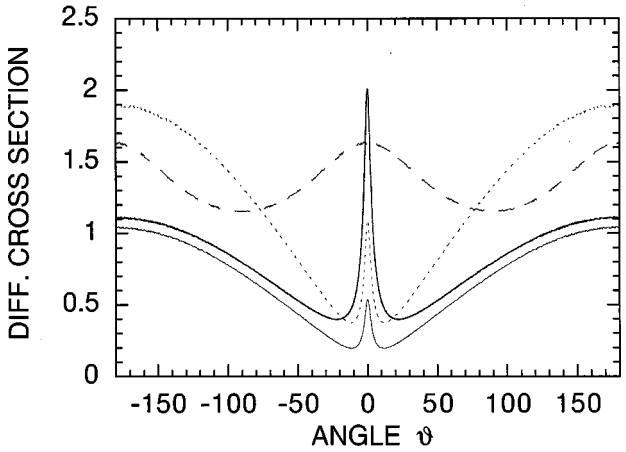

FIG. 8. Summed differential cross sections $d\sigma/do$ scaled in 10^{-14} a.u. of ± 100 peaks around the elastic one as a function of the angle ϑ for an electrical field strength of $E=5.89$ a.u. The electron energy is $W=4\times c^2$, and the relativistic parameter is $\gamma=5$. The thick solid line denotes the complete result for electrons, the short dashed one sketches the values for spinless particles, and the long dashed one is the result for the nonrelativistic limit. The thin line is the contribution from the free bispinor part of the Volkov wave function.

V. CONCLUSION

The motivation of this study of Mott scattering in an ultrastrong laser field was to discuss the main properties of a well-characterized laser-assisted collision process, in which relativistic effects are expected to play a prominent role. To this end, we have compared, for a representative scattering geometry, the results obtained from the full Dirac-Volkov calculation with those derived from simpler approaches, namely, for a spinless (Klein-Gordon) projectile and for a nonrelativistic electron.

A first general result has been to show explicitly that, for large-angle scattering geometries, a low-frequency infrared laser can be remarkably effective for redistributing, via stimulated emission and absorption of laser photons, the projectile kinetic energy over a very wide range. The distribution in energy of the outgoing electrons at a fixed scattering angle is approximately centered on the incoming energy, i.e., on the elastic peak, corresponding to zero net exchange of photons with the field. As a typical example, for a Nd laser with angular frequency $\omega=1.17$ eV and scattering angle $\eta=\pi/2$, the spread toward positive energy transfers can extend up to about 27 000 photons for an electrical field strength $E=1$ a.u. and a projectile kinetic energy $W_{\mathrm{kin}}=2.7$ keV, up to about 523 000 for an electrical field strength $E=5.89$ a.u. and a projectile kinetic energy $W_{\mathrm{kin}}=510.7$ keV. This entails a considerable decrease of the magnitude of the differential scattering cross section with exchange of a given net number pf photons, as compared to the field-free elastic cross section, more precisely, for $n=0$ the ratio between the laser-assisted and the field-free elastic cross sections can be estimated as being of the order of $|J_0(\zeta)|^2 \leqslant 2/\pi\zeta$. If the energy of the incoming electron is high enough, the loss in the elastic peak is evenly spread between stimulated emission and absorption processes, which can be identified as stimulated bremsstrahlung and stimulated inverse bremsstrahlung, respectively. A notice-

able asymmetry in the energy distribution is observed, which can be ascribed to kinematical factors depending on the scattering geometry. Another source of asymmetry also comes from the fact that the final energy of the projectile is bounded from below to zero. This situation arises if the incoming projectile energy is not high enough as compared to the maximum number of photons, which can be emitted in the process. Although stimulated recombination could in principle take place, the system ending in a bound hydrogenic state, we did not discuss this process here as it plays only a marginal role.

The kinetic-energy spectrum of the scattered electrons, which replicates the distribution of the net number of exchanged photons, always exhibits a sharp decrease beyond a quite well-defined cutoff. The location of the cutoff is an important physical parameter which characterizes the maximum amount of energy which can be exchanged between the projectile and the field. It can be estimated via a rather simple classical analysis wich singles out the importance of terms related to the net momentum transfer taking place in the course of the collision. More precisely, the width of the distribution is related not only to the averaged ponderomotive energy gained by the electron in the field but also to its transient energy. The pertinence of the analysis is confirmed by comparing to a quantum approach where the relevant parameter is then the momentum dependence contained in the argument of the Bessel function $J_n(\zeta)$. J_n represent in some sense the relative weights of a dressed stated with energy and momenta shifted in the presence of n photons from the laser field. The maximum energy transfer then coincides with the limit $n \simeq \zeta$, beyond which, for larger values of n, the Bessel functions decrease exponentially. Our analysis confirms the concordance of the two pictures, which both provide a fair estimate of the width of the distribution.

For relatively slow projectiles with a kinetic energy of 2.7 keV, we have verified that the three approaches considered here [nonrelativistic, relativistic spinless (Klein-Gordon), and Dirac-Volkov] lead to almost indistinguishable results at rather low laser intensities of about 10^{13} W/cm^2. However, relativistic effects induced by the laser start to show up already at a field strength of $E=1$ a.u. (corresponding to 3.5×10^{16} W/cm^2). A clear signature is the change in the position of the high-energy cutoff, which is shifted toward higher energies by about 200ω as compared to the nonrelativistic calculation. For such conditions differences between the Klein-Gordon and Dirac treatments are negligible, as expected.

Even stronger electrical field strengths reveal significant differences between the two relativistic treatments. While in most cases the contribution from the free bispinor part of the Volkov wave function turns out to be dominant, for higher field strengths and faster projectiles the contributions of the spin-dependent terms significantly increase the differential cross section in the propagation direction $\vec{k}$ of the laser. These contributions, which arise from the coupling between the spin and the field, become dominant at higher field strength, thus demonstrating that a complete Dirac-Volkov electron treatment is necessary in this regime.

ACKNOWLEDGMENTS

C.S. acknowledges financial support from the German Academic Exchange Service (Doktorandenstipendium HSP II/AUFE). C.H.K. was supported financially by the U.K. Engineering and Physical Sciences Research Council. This research was supported as well in part by the European Union through Contract No. CRB CHRX CT 940470. The Laboratoire de Chimie Physique—Matière et Rayonnement is Unité de Recherche Associée au CNRS (URA 176).

APPENDIX

In order to average over initial and final polarizations, a factor $\frac{1}{2}$ and a summation over final and initial polarization states of the electron has to be included. In the calculation of the differential cross section $d\sigma$, the squared modulus of products of γ matrices and dyadics $(u\overline{u})=c\not{p}+c^2$ of bispinors arise from the matrix element $T_{f\leftarrow i}$. Due to the well-known identity

$$\sum_{i,f} |\overline{u'}\ldots\gamma\ldots u|^2 = \mathrm{Tr}[\ldots\gamma\ldots(u'\overline{u'})\ldots\gamma\ldots(u\overline{u})], \tag{A1}$$

where i and f count, respectively, initial and final polarization states, the averaging can be reduced to the calculation of traces of γ-matrices. In expression (21) derived above there are 36 products of this form to be evaluated.

In the following formulas the abbreviation $\tilde{x}^\mu=(v^0,-\vec{v}^i)$ is used. This has proven to be convenient in describing the action of the adjoint γ matrices like $(\gamma^\dagger v)=(\gamma\tilde{v})$ and the signs arising from commutation operations between γ^0 and γ^μ inside the different traces due to $\{\gamma^0,\gamma^\mu\}=2g^{0\mu}$.

First, there are four contributions multiplied by the prefactor $|B_n|^2=J_n(\zeta)^2$: The modulus of the contribution containing the Mott spin factor reduces to

$$\mathrm{Tr}[\gamma^0(c\not{p}'+c^2)\gamma^0(c\not{p}+c^2)]=4c^2[c^2+(p\tilde{p}')], \tag{A2}$$

the modulus of the contribution from the A^2 term becomes

$$\mathrm{Tr}[\not{k}\gamma^0\not{k}(c\not{p}+c^2)\not{k}\gamma^0\not{k}(c\not{p}'+c^2)]=32(kp)(kp')\omega^2, \tag{A3}$$

and the two interference terms between them yield

$$\begin{aligned}&\mathrm{Tr}[\gamma^0(c\not{p}+c^2)\not{k}\gamma^0\not{k}(c\not{p}'+c^2)]\\&\quad+\mathrm{Tr}[\not{k}\gamma^0\not{k}(c\not{p}+c^2)\gamma^0(c\not{p}'+c^2)]\\&=16\omega^2c^2+16\omega^2(p\tilde{p}')+8c^2(kp')(kp)-8c^2(k\tilde{p}')(k\tilde{p}).\end{aligned} \tag{A4}$$

Second, the 16 contributions multiplied by the prefactors are mutually complex conjugates according to

$$\begin{aligned}&Bc_n(\zeta,\phi_0)^*B_n(\zeta,\phi_0)+Bc_n(\zeta,\phi_0)B_n(\zeta,\phi_0)^*\\&\quad=[J_n(\zeta)J_{n+1}(\zeta)+J_n(\zeta)J_{n-1}(\zeta)]\cos\phi_0\end{aligned} \tag{A5}$$

are considered similarly for Bs_n. Noting that $\not{k}\gamma^0\not{k}=2\omega^2/c^2(\gamma^0-\gamma^3)$, there are two traces in arising from the A^2 term which have similar structures:

$$\begin{aligned}&\mathrm{Tr}[\not{A}_i\not{k}\gamma^0(c\not{p}+c^2)\gamma^0(c\not{p}'+c^2)]\\&\quad=4c^2[(A_ip')(k\tilde{p})-(A_i\tilde{p})(kp')]\end{aligned} \tag{A6}$$

and

$$\mathrm{Tr}[\not{A}_i \not{k} \gamma^0 (c\not{p}+c^2)\gamma^3(c\not{p}'+c^2)] = 4c^2[-(A_i p)(kp')+(A_i p')(k\tilde{p})], \tag{A7}$$

where $i \in \{x,y\}$, which also appear with interchanged initial and final momenta $p \leftrightarrow p'$. It is realized that the first trace is to be calculated as well for the contribution containing the Mott factor.

Finally, there are 16 contributions multiplied by $|Bc_n(\zeta,\phi_0)|^2$ and $|Bs_n(\zeta,\phi_0)|^2$, respectively. The eight cross terms between contributions from A_x and A_y vanish, which was expected because they do not describe a physical situation but arise from the chosen description of the circular polarization in Cartesian components. Now there are two different traces to be evaluated, where again $i \in \{x,y\}$ is used, and they read

$$\mathrm{Tr}[\not{k}\not{A}_i(c\not{p}'+c^2)\not{A}_i\not{k}(c\tilde{\not{p}}+c^2)] = -8c^2A_i^2(kp')(k\tilde{p}) \tag{A8}$$

and

$$\mathrm{Tr}[\tilde{\not{k}}\tilde{\not{A}}_i(c\tilde{\not{p}}'+c^2)\not{k}\not{A}_i(c\not{p}+c^2)] + \mathrm{Tr}[\not{k}\not{A}_i(c\tilde{\not{p}}'+c^2) \times \tilde{\not{k}}\tilde{\not{A}}_i(c\not{p}+c^2)] = 16\omega^2\left\{\tilde{A}_iA_i\frac{c^2}{2\omega^2}[(kp)(kp')+(k\tilde{p})(k\tilde{p}')]+[(A_ip') \times(A_ip)+(A_i\tilde{p})(A_i\tilde{p}')]-A_i\tilde{A}_i[c^2+(p\tilde{p}')]\right\}. \tag{A9}$$

[1] See, for instance, *High-Field Interactions and Short-wavelength Generation*, edited by H. Milchberg and R. Freeman, special issue of J. Opt. Soc. Am. B **13**, 51 (1996); **13**, 314 (1996).

[2] L. S. Brown and T. W. B. Kibble, Phys. Rev. **133**, A705 (1964); T. W. B. Kibble, *ibid.* **138**, B740 (1965); **150**, 1060 (1966); J. H. Eberly and H. R. Reiss, Phys. Rev. **145**, 1035 (1966); H. R. Reiss and J. H. Eberly, *ibid.* **151**, 1058 (1966); J. H. Eberly and A. Sleeper, *ibid.* **176**, 1570 (1968).

[3] I. I. Goldman, Phys. Lett. **8**, 103 (1964); Zh. Éksp. Teor. Fiz. **46**, 1412 (1964) [Sov. Phys. JETP **19**, 954 (1964)]; A. I. Nikishov and V. I. Ritus, *ibid.* **46**, 776 (1964); [*ibid.* **19**, 529 (1964)]; **46**, 1768 (1964) [**19**, 1191 (1964)]; N. B. Narozhny, A. I. Nikishov, and V. I. Ritus, *ibid.* **47**, 930 (1964) [*ibid.* **20**, 622 (1965)].

[4] V. B. Berestetzkiĭ, E. M. Lifshitz, and L. P. Pitaevskiĭ, *Quantum Electrodynamics*, 2nd ed. (Pergamon, Oxford, 1982).

[5] C. I. Moore, J. P. Knauer, and D. D. Meyerhofer, Phys. Rev. Lett. **74**, 2439 (1995).

[6] P. Monot, T. Auguste, P. Gibbon, F. Jakober, G. Mainfray, A. Dulieu, M. Louis-Jacquet, G. Malka, and J. L. Miquel, Phys. Rev. Lett. **74**, 2953 (1995).

[7] C. Bula, K. T. McDonald, E. J. Prebys, C. Bamber, S. Boege, T. Kotseroglou, A. C. Melissinos, D. D. Meyerhofer, W. Ragg, D. L. Burke, R. C. Field, G. Horton-Smith, A. C. Odian, J. E. Spencer, D. Walz, S. C. Berrigde, W. M. Bugg, K. Shmakov, and A. W. Weidemann, Phys. Rev. Lett. **76**, 3116 (1996).

[8] L. Rosenberg, Phys. Rev. A **49**, 1122 (1994).

[9] M. V. Fedorov, S. P. Goreslavsky, and V. S. Letokhov, Phys. Rev. E **55**, 1015 (1997).

[10] E. S. Sarachik and G. T. Schappert, Phys. Rev. D **1**, 2738 (1970); Y. I. Salamin and F. H. M. Faisal, Phys. Rev. A **54**, 4383 (1996).

[11] P. A. Norreys, M. Zepf, S. Moustaizis, A. P. Fews, P. Lee, M. Bakarezos, C. N. Danson, A. Dyson, P. Gibbon, P. Loukakos, D. Neely, F. N. Walsh, J. S. Wark, and A. E. Dangor, Phys. Rev. Lett. **76**, 1832 (1996); D. von der Linde, T. Engers, G. Jenke, P. Agostini, G. Grillon, E. Nibbering, A. Mysyrowicz, and A. Antonetti, Phys. Rev. A **52**, R25 (1995).

[12] Y. L. Shao, T. Ditmire, J. W. G. Tisch, E. Springate, J. P. Marangos, and M. H. R. Hutchinson, Phys. Rev. Lett. **77**, 3343 (1996); T. Ditmire, J. W. G. Tisch, E. Springate, M. B. Mason, N. Hay, J. P. Marangos, and M. H. R. Hutchinson, *ibid.* **78**, 2732 (1997); T. Ditmire, J. W. G. Tisch, E. Springate, M. B. Mason, N. Hay, R. A. Smith, J. P. Marangos, and M. H. R. Hutchinson, Nature (London) **386**, 54 (1997).

[13] F. V. Bunkin and M. V. Fedorov, Zh. Éksp. Teor. Fiz. **49**, 1215 (1965) [Sov. Phys. JETP **22**, 844 (1966)].

[14] N. M. Kroll and K. M. Watson, Phys. Rev. A **8**, 804 (1973).

[15] F. E. Low, Phys. Rev. **110**, 974 (1958).

[16] A. Weingartshofer, J. K. Holmes, G. Laudie, E. M. Clarke, and H. Krüger, Phys. Rev. Lett. **39**, 269 (1977); A. Weingartshofer, J. K. Holmes, J. Sabdagh, and S. L. Chin, J. Phys. B **16**, 1805 (1983), and references therein.

[17] N. F. Mott, Proc. R. Soc. London Ser. A **124**, 425 (1929); **135**, 429 (1932); W. A. McKinley and H. Feshbach, Phys. Rev. **74**, 1739 (1948).

[18] F. V. Hartemann and A. K. Kerman, Phys. Rev. Lett. **76**, 624 (1996); F. V. Hartemann and N. C. Luhmann, *ibid.* **74**, 1107 (1995).

[19] M. M. Denisov and M. V. Fedorov, Zh. Éksp. Teor. Fiz. **53**, 1340 (1967) [Sov. Phys. JETP **26**, 779 (1968)].

[20] J. Z. Kamiński, J. Phys. A **18**, 3365 (1985).

[21] F. Zhou and L. Rosenberg, Phys. Rev. A **45**, 7818 (1992).

[22] F. Zhou and L. Rosenberg, Phys. Rev. A **48**, 505 (1993).

[23] S. P. Roshchupkin, Zh. Éksp. Teor. Fiz. **109**, 337 (1996) [Sov. Phys. JETP **82**, 177 (1996)].

[24] C. H. Keitel and P. L. Knight, Phys. Rev. A **51**, 1420 (1995); C. H. Keitel, P. L. Knight, and K. Burnett, Europhys. Lett. **24**, 539 (1993).

[25] C. H. Keitel, J. Phys. B **29**, L 873 (1996).

[26] M. Protopapas, C. H. Keitel, and P. L. Knight, J. Phys. B **29**, L591 (1996).

[27] F. H. M. Faisal and T. Radożycki, Phys. Rev. A **47**, 4464 (1993); **48**, 554 (1993).

[28] O. Latinne, C. J. Joachain, and M. Dörr, Europhys. Lett. **26**, 333 (1994).

[29] E. S. Fradkin, D. M. Gitman, and Sh. M. Shvartsman, *Quantum Electrodynamics with Unstable Vacuum* (Springer, Berlin, 1991).
[30] D. M. Volkov, Z. Phys. **94**, 250 (1935).
[31] J. J. Sakurai, *Advanced Quantum Mechanics* (Addison-Wesley, Reading, MA, 1967).
[32] J. D. Bjorken and S. D. Drell, *Relativistic Quantum Mechanics* (McGraw-Hill, New York, 1964); C. Itzykson and J.-B. Zuber, *Quantum Field Theory* (McGraw-Hill, New York, 1985).
[33] F. W. J. Olver, in *Handbook of Mathematical Functions*, edited by M. Abramowitz and I. A. Stegun, 5th ed. (Dover, New York, 1968).